MHD Simulations of Flares

Takaaki YOKOYAMA
National Astronomical Observatory, Nobeyama, Minamimaki, Minamisaku, Nagano 384-1305, Japan
E-mail: yokoyama@solar.mtk.nao.ac.jp

Abstract

A two-dimensional simulation of a solar flare is performed using a magnetohydrodynamic (MHD) code including nonlinear anisotropic heat conduction effect. The flare energy is released by the magnetic reconnection mechanism stimulated initially by the resistivity perturbation in the corona. The released thermal energy is transported into the chromosphere by heat conduction and drives chromospheric evaporation. Temperature and derived soft X-ray distributions are similar to the cusp-like structure of long-duration-event (LDE) flares observed by the soft X-ray telescope aboard Yohkoh satellite. Density and radio free-free intensity maps show a simple loop configuration which is consistent with the observation with Nobeyama Radio Heliograph.

Key words: Flare — MHD simulation — Conduction

1. Introduction

Magnetic reconnection is now believed to be the energy release mechanism for a solar flare (Carmichael 1964; Sturrock 1966; Hirayama 1974; Kopp & Pneuman 1976). Figure 1. shows this model (also including the newly found facts by our numerical simulations). In this model, the energy of coronal field is released around the magnetic X-point. The released energy is converted to become thermal and kinetic energy of the coronal plasma. The observation of cusp-shape loops in soft X-ray (Tsuneta et al. 1992) and hard X-ray sources above soft X-ray loops (Masuda et al. 1994) both support this model because these observation suggest the primary site of the energy release above the soft X-ray loops. The discovery of escaping plasmoids from flare sites (Shibata et al. 1995; Ohyama & Shibata 1997) is additional evidence for this model because the theory predicts ejection of plasma from the reconnection site. So-called "chromospheric evaporation" (Neupert 1968) that is observed as a blue-shift of the X-ray lines is thought to be an ablation of chromospheric plasma by the energy released through reconnection and transported by heat conduction and/or by non-thermal electrons during a flare and that is another piece of indirect support for the magnetic reconnection model. In this paper we show our study of the reconnection and the chromospheric evaporation by means of a two-dimensional MHD simulation using the newly developed numerical code including nonlinear anisotropic heat conduction effect (Yokoyama & Shibata 1997, 1998).

2. Simulation Models and Results

We solve the two-dimensional, nonlinear, time-dependent, resistive, compressible MHD equations. Gravitational acceleration is ignored. Ohmic heating and heat conduction effects are taken into account. The conduction coefficient is the Spitzer-type one which is proportional to $T^{5/2}$ where T is temperature, working only in the direction along the magnetic field line. The initial plasma is in magnetohydrostatic equilibrium with antiparallel magnetic fields, between which a current sheet is situated (Fig. 2.). The units of length, velocity, and time in the simulations are $\delta = 3000$ km, $C_{s0} = 170$ km s^{-1}, and $\tau \equiv \delta/C_{s0} \approx 18$ s, respectively, where δ and C_{s0} are the thickness of the initial current sheet and the sound speed of the initial coronal plasma. Density and temperature are normalized with the initial coronal values $n_0 = 10^9$ cm^{-3} and $T_0 = 2 \times 10^6$ K, respectively. The initial plasma beta $\beta = 0.2$ are uniform everywhere except for the current sheet region. We took a dense and low-temperature region located in $z < 1$ for modeling the chromosphere, the density of which is 10^5 times of the coronal one. The initial equilibrium is perturbed by a finite resistivity in $t \leq t_i = 2$ in a localized spot at $(x, z) = (0, 20)$ in the current sheet. For $t > t_i$ the resistivity is determined self-consistently from the local value of the current density for every time step. The sound-crossing time $\tau \equiv \delta/C_{s0} \approx 18$ s, the Alfvén-crossing time $\tau_A \equiv \delta/V_A \approx 7.4$ s, and the heat conduction time $\tau_c \equiv \delta^2(n_0 k_B/\kappa) \approx 2.2$ s. Thus, the conduction time is shorter than the Alfvén-crossing time.

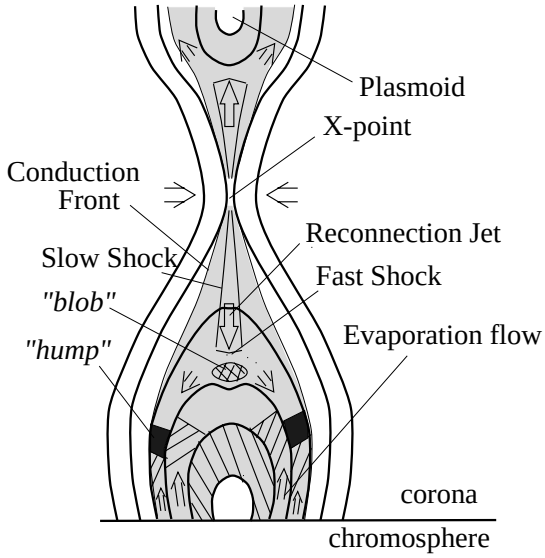

Fig. 1.. Schematic illustration of the magnetic reconnection model of a flare (Carmichael 1964; Sturrock 1966; Hirayama 1974; Kopp & Pneuman 1976). Also included is our simulation results. Thick solid lines show magnetic field lines. The hatched region has a higher temperature than the ambient corona during the flare.

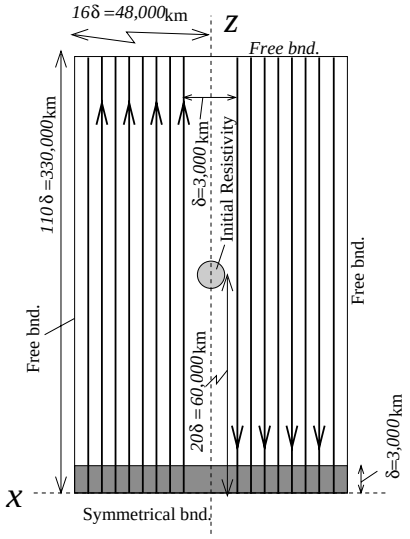

Fig. 2.. Computation model of the simulation of a flare. Solid lines indicate the magnetic field. The hatched area near the x axis is the dense region simulating the chromosphere.

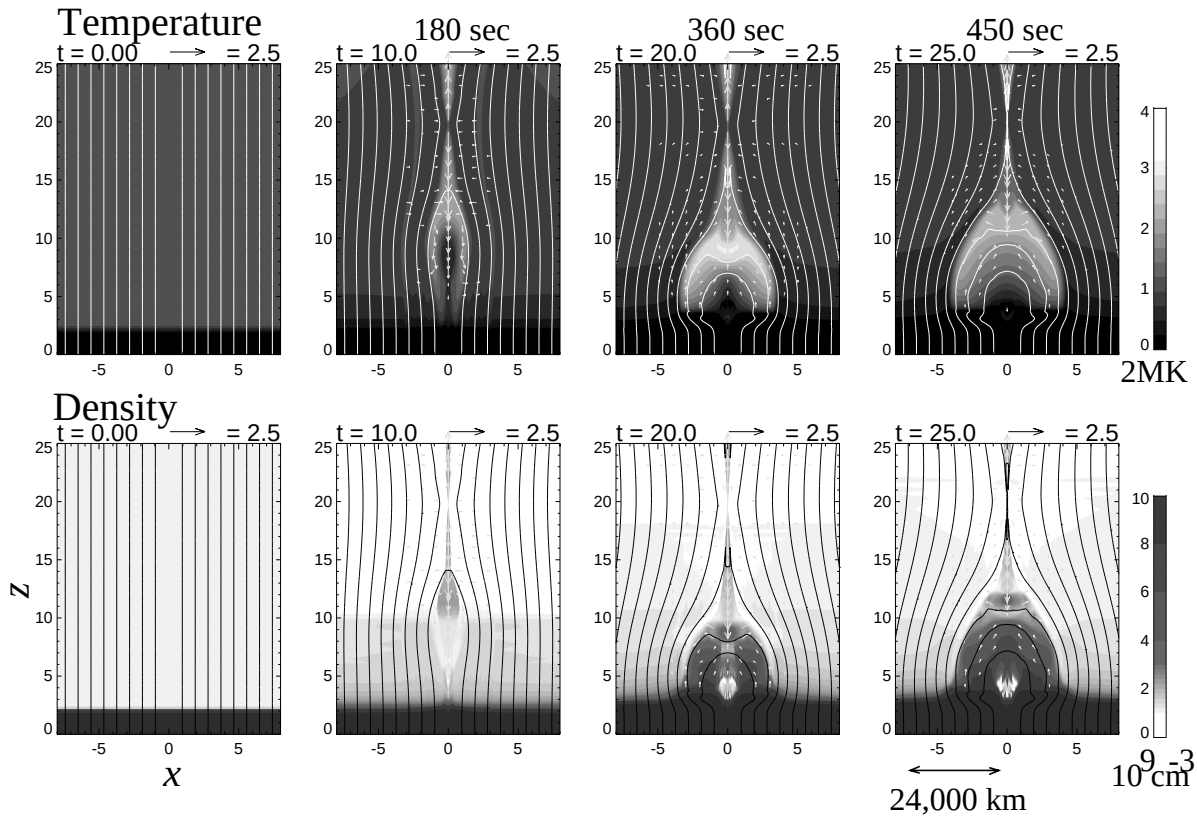

Fig. 3.. Results of the simulation. Upper and lower panels show the temporal evolution of temperature and density distribution, respectively. The arrows represent the velocity, and lines show the magnetic field lines. The unit of length, velocity, time, temperature, and density is 3000 km, 170 km s^{-1}, 18 s, 2×10^6 K, and 10^9 cm^{-3}, respectively. In the initial condition ($t = 0$) a dense region is located near the bottom of the simulation box in which the density is about 10^5 times that of the other region.

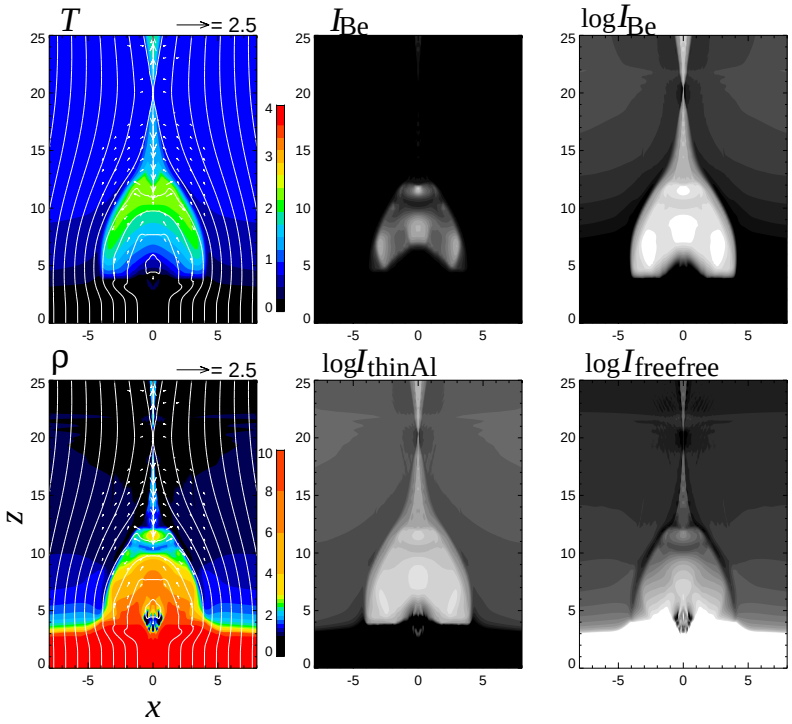

Fig. 4.. X-ray and radio maps derived from the simulation results. For the X-ray map, the response of the filter attached to the soft X-ray telescope on board *Yohkoh* is taken into account. $I_{\rm Be}$ and $I_{\rm thinAl}$ are the intensity through the beryllium and the thin aluminum filters. The radio map $I_{\rm freefree}$ is derived under the assumption that the emission is by the thermal free-free mechanism. The unit of intensity is arbitrary.

Figure 3. shows the results. Because of the enhanced resistivity, the point $z = 20$ in the current sheet evolves to an X-point of the magnetic reconnection ($t = 10$). The reconnected field lines together with the frozen-in plasma are ejected as upward and downward jets from this X-point due to the magnetic tension force. *Slow-mode MHD shocks* are formed at the boundary between the inflows and the outflows.

In the temperature distribution at $t = 20$ in Fig. 3., a clear cusp shape is seen. The outer edge of this cusp is a pair of the *conduction fronts* propagating from the X-point. The conduction fronts transport the thermal energy, which is released at the slow-mode shocks in this region, along the field lines and form the cusp shape of hot plasma. Note that the global cusp shape of the hot region behind the conduction front is similar to the soft X-ray solar flare loops in long-duration (LDE) flares (Tsuneta et al. 1992). Since the conduction front propagates faster than the inflow of the shock, the temperature jump between the inflow and the outflow is smoothed away. The jumps in the density distribution at $t = 20$ in Fig. 3. is, therefore, *isothermal slow-mode MHD shocks*.

The reconnected magnetic field which goes down from the X-point finally forms a closed loop ($t = 25$ in Fig. 3.). In the density distribution, a growing plasma mound can be seen in the panels of $t = 20$ and $t = 25$ of Fig. 3.. This is a direct consequence of the chromospheric evaporation. The velocity of the evaporation flow is $V_{\rm ev} = 0.2$–0.4 and is 0.2–0.3 times the local sound speed. The density of the evaporated plasma is ≈ 10 times the initial coronal density at maximum and ≈ 5 times in average.

The evolution from the rise phase to (the early part of) the decay phase of a solar flare should be reproduced in this simulation. We 'observe' the computation results under the response of real X-ray instruments. It is compared with real flares on the Sun. Figure 4. shows the derived images from the 'observation' of the simulation results after taking into account of the response of the beryllium and the thin aluminum filters of the *Yohkoh* soft X-ray telescope (Tsuneta et al. 1991). The X-ray distribution is very similar to the observed cusp-like structure of loops of long-duration-event (LDE) flares (Tsuneta et al. 1992). Also shown in Figure 4. is the thermal free-free emission of the plasma which should be observed with the radio telescopes. The calculated shape of the bright region in radio is loop-like because the thermal emission is stronger from the cool plasma in the evaporation flow than from the hot plasma in the cusp. This result is consistent with the Nobeyama Radio Heliograph observation which showed a

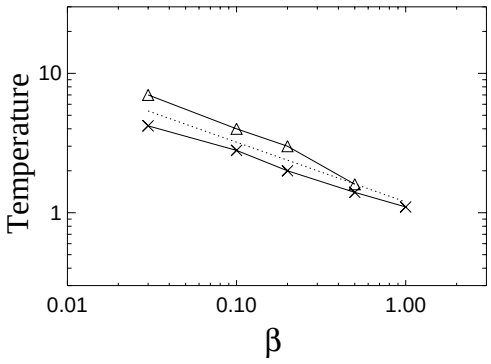

Fig. 5.. Dependence of the flare temperature on the initial plasma $\beta \equiv p/p_{\rm m}$, where p and $p_{\rm m}$ are gas and magnetic pressures respectively. Triangles are the temperature at the loop top behind the fast-mode shock, and crosses are the averaged temperature in the loop. The dotted line is the theoretical result derived from equation (4) in the text. When $\beta \geq 1$, no fast-mode shock forms and so no data point is shown.

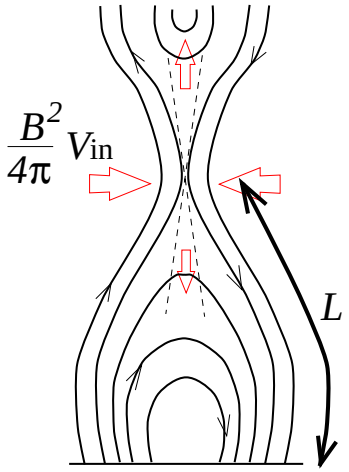

Fig. 6.. Sketch of the flare loop for explaining the new scaling law.

simple loop structure in radio image of the LDE flare with an X-ray cusp (Hanaoka 1994). It is noted that the outer edge of the cusp structure is the conduction fronts, *not* the slow-mode MHD shocks. It is also pointed out that there is a dip in the temperature distribution at the loop top formed by the penetration of the reconnection jet into the closed loops. This is similar to the observed temperature distribution of the impulsive flare (Tsuneta et al. 1997).

3. Scaling Law of Flare Temperature

One of the interesting questions relating to flares is, "What determines the flare temperature and its distribution ?" We performed several simulation runs and found an interesting scaling law between the initial coronal plasma beta β and the flare temperature. That is

$$T_{\rm A} \propto \beta^{-6/7},$$

where $T_{\rm A}$ is the temperature at the flare loop apex (Fig. 5.). This relation can be explained as follows. If we assume that the input of energy to a loop balances with the conduction cooling rate, we obtain

$$\kappa_0 T_{\rm A}^{7/2}/L^2 \approx Q, \tag{1}$$

and then, the temperature at the loop apex is

$$T_{\rm A} \approx (2QL^2/\kappa_0)^{2/7} \tag{2}$$

where Q is the volumetric heating rate, L is the half-length of the loop and κ_0 is the heat conduction coefficient (Figure 6.; Fisher & Hawley 1990). In our simulations, the heating mechanism is magnetic reconnection so that the heating rate is described as

$$Q = B^2/(4\pi) \cdot V_{\rm in}/L \cdot 1/\sin\theta, \tag{3}$$

where $V_{\rm in}$ is the inflow velocity ($\approx 0.1 V_{\rm A}$ from our result), and θ is the angle between the slow-mode MHD shock and the loop and is approximately given by $\sin\theta \approx V_{\rm in}/V_{\rm A}$. By manipulating these, we find

$$T_{\rm A} \approx \left(\frac{B^3 L}{2\pi\kappa_0\sqrt{4\pi\rho}}\right)^{\frac{2}{7}} \propto B^{\frac{6}{7}} \propto \beta^{-\frac{3}{7}}, \tag{4}$$

where ρ is the coronal density. The simulation results (Fig. 5.) show very good agreement with this scaling law. When $\beta = 0.01$ that is the typical value in the real solar corona, this scaling law predicts the flare temperature $T \approx 10$ MK (see also Fig. 5.), which is consistent with the observed flare temperature $T \approx 10$–20 MK (e.g. Tsuneta et al. 1992).

The computations were carried out on the supercomputers at NAOJ.

References

Carmichael H. 1964, in *Proc. of AAS-NASA Symp. on the Physics of Solar Flares*, ed. W. N. Hess, (NASA Spec. Pub. 50) p451

Fisher G. H., Hawley S. L. 1990, ApJ 357, 243

Hanaoka Y. 1994, in *Procs. of Kofu Symp., New Look at the Sun with Emphasis on Advanced Observations of Coronal Dynamics and Flares*, eds. S. Enome & T. Hirayama (NRO Report No.360) p181

Hirayama T. 1974, Sol. Phys. 34, 323

Kopp R. A., Pneuman G. W. 1976, Sol. Phys. 50, 85

Masuda S., Kosugi T., Hara T., Tsuneta S., Ogawara Y. 1994, Nature 371, 495.

Neupert W. M. 1968, ApJ 153, L59

Ohyama M., Shibata K. 1997, PASJ 49, 249.

Shibata K., Masuda S., Shimojo M., Hara H., Yokoyama T., Tsuneta S., Kosugi T., Ogawara Y. 1995, ApJ 451, L83.

Sturrock P. A. 1966, Nature 211, 695

Tsuneta S., Acton L., Bruner M., Lemen J., Brown W., Caravalho R., Catura R., Freeland S., Jurcevich B., Morrison M., Ogawara Y., Hirayama T., Owens J. 1991, Sol. Phys. 136, 37

Tsuneta S., Hara H., Shimizu T., Acton L. W., Strong K. T., Hudson H. S., Ogawara Y. 1992, PASJ 44, L63

Tsuneta S., Masuda S., Kosugi T., Sato J. 1997, ApJ 478, 787.

Yokoyama T., Shibata K. 1997, ApJ 474, L61

Yokoyama T., Shibata K. 1998, ApJ 494, L113